A furnace design for XANES spectroscopy of silicate melts under controlled oxygen fugacities and temperatures to 1773 K

Andrew J. Berry,[a]* J. Michael G. Shelley,[a] Garry J. Foran,[b,c] Hugh St. C. O'Neill[a] and Dean R. Scott[a]

[a]Research School of Earth Sciences, Australian National University, Canberra, ACT 0200, Australia, [b]Australian Synchrotron Research Program, Australian Nuclear Science and Technology Organisation, PMB 1, Menai, NSW 2234, Australia, and [c]Australian National Beamline Facility, KEK, Photon Factory, Oho 1-1, Tsukuba-shi, Ibaraki-ken 305-0801, Japan. E-mail: andrew.berry@anu.edu.au

A controlled-atmosphere furnace has been constructed for X-ray absorption spectroscopy experiments under imposed oxygen fugacities at temperatures up to 1773 K. The use of the furnace is demonstrated in a study of the oxidation state of Cr in a basaltic silicate melt (mid-ocean ridge basalt) by *K*-edge XANES spectroscopy. This is the first time the Cr^{2+}/Cr^{3+} ratio has been identified directly in an Fe-bearing melt. At typical terrestrial oxygen fugacities around half the Cr is present as Cr^{2+}, even though this oxidation state has never been identified in a terrestrial material and only Cr^{3+} is observed after quenching to a glass. Cr^{2+} oxidizes to Cr^{3+} on cooling in the presence of Fe^{3+} according to the electron exchange reaction $Cr^{2+} + Fe^{3+} \rightarrow Cr^{3+} + Fe^{2+}$. This illustrates the importance of the *in situ* determination of metal oxidation states in melts.

Keywords: spectroscopy furnaces; XANES; controlled oxygen fugacity; oxidation states; silicate melts; mid-ocean ridge basalts.

1. Introduction

The abundance of elements in a naturally occurring silicate melt (magma) can be used to constrain variables associated with the formation of a magma by partial melting and its subsequent evolution through processes such as fractional crystallization. Integral to understanding the abundance of an element is the way in which it partitions between crystals and coexisting melt. For multiple valence elements, partitioning is strongly dependent upon the oxidation state and is hence also a sensitive indicator of redox conditions or oxygen fugacity (fO_2).

The oxidation states determined from room-temperature studies of quenched melts (*i.e.* glasses) do not necessarily correspond to those present in a melt at high temperature due to the possibility of disproportionation or charge-transfer reactions on cooling. In a melt, multiple oxidation states may be stabilized by entropy (*e.g.* V^{3+}, V^{4+} and V^{5+} or U^{4+}, U^{5+} and U^{6+}). On rapid cooling (minutes to hours) the diffusion of O_2 into or out of a melt will not occur (closed system with respect to O_2 content), however, variable redox species may still re-equilibrate as a function of temperature since charge-transfer reactions only involve the redistribution of electrons. At low temperatures, the total number of multiple-element oxidation states should approach the minimum required to account for the oxygen content of the system. As a result of re-equilibration by electron exchange, at room temperature the most abundant redox variable element will occur in two oxidation states (usually Fe^{2+} and Fe^{3+} in natural magmas) and the minor elements in just one (unless the potentials of the minor element redox couples relative to Fe are very similar). Above the glass transition temperature electron exchange reactions may be facilitated by mobility of the redox active species. At lower temperatures the cations involved may need to occupy adjacent sites. For basaltic melts (containing ~10 wt% FeO) a minor element will statistically always have at least one Fe cation as a next nearest neighbour. The high-temperature distribution of species may not be quenchable due to the rapid nature of electron-transfer reactions associated with re-equilibration. It is therefore important to study the melts *in situ.* X-ray absorption near-edge structure (XANES) spectroscopy can be used to determine and quantify oxidation states from changes in the energy and/or intensity of edge features (Waychunas *et al.*, 1983; Waychunas, 1987). In general terms, pre-edge transitions (such as $1s \rightarrow 3d$) and the main absorption edge shift to higher energy with increasing oxidation state (Wong *et al.*, 1984; Sutton *et al.*, 1993; Bajt *et al.*, 1994). Pre-edge features typically shift ~1 eV/charge while shifts of >3 eV/charge may occur for absorption edges comprising transitions to weakly bound states (such as $1s \rightarrow 4p$).

As an example, Cr is an element of potentially variable oxidation state in magmas but which is only found as Cr^{3+} in the source rocks or samples cooled from the melt. In Fe-free silicate melts equilibrated under typical terrestrial fO_2s, Cr occurs as both Cr^{3+} and Cr^{2+} (Schreiber & Haskin, 1976), but Cr^{2+} is not found in Fe-bearing glasses quenched from similar conditions. There is also indirect evidence for Cr^{2+} in Fe-bearing silicate melts from both crystal-melt partitioning experiments (Barnes, 1986; Murck & Campbell, 1986; Roeder & Reynolds, 1991; Hanson & Jones, 1998; Poustovetov & Roeder, 2000) and the high Cr content of some natural olivines (Li *et al.*, 1995). Cr^{2+} has never been identified in a terrestrial material and it has been considered impossible to determine directly Cr oxidation states in Fe-bearing melts (Poustovetov & Roeder, 2000). XANES spectroscopy has identified Cr^{2+} in lunar olivine (Sutton *et al.*, 1993) and here we use this technique to investigate Cr oxidation states at high temperatures in silicate melts.

A number of designs for X-ray spectroscopy furnaces have been reported previously. In most cases the sample is heated in a vacuum (Waychunas *et al.*, 1988; Farges *et al.*, 1999; Filipponi *et al.*, 2000), air (Farges *et al.*, 1994, 1996; Dent *et al.*, 1995) or an inert gas environment (Crozier *et al.*, 1977; Lytle *et al.*, 1979; Jackson *et al.*, 1993). Fe oxidation states in geological melts have been controlled over a limited range by adjusting the oxygen partial pressure with a vacuum (Waychunas *et al.*, 1988) or using flowing nitrogen in a furnace with Mo components to produce an fO_2 near the Mo/MoO_2 buffer (Jackson *et al.*, 1993). The use of CO/CO_2 and N_2/air gas mixtures to control fO_2 at temperatures up to ~1500 K has also been reported (Hoser *et al.*, 1995; Hilbrandt & Martin, 1999). In some designs a vacuum or inert gas is required to prevent oxidation of the furnace heating element (Farges *et al.*, 1995; Filipponi *et al.*, 2000); metals such as Ir, W and Ta can be used to achieve temperatures in excess of 3300 K. Reactive samples can be supported without contact by both electromagnetic and gas flow levitation (Jacobs *et al.*, 1996; Launay *et al.*, 1997). High pressures in conjunction with high temperatures have been achieved using autoclave, Paris–Edinburgh and diamond-anvil type cells [see Filipponi (2001) for a review]. Flowing gas environments designed to control the chemistry of a sample have been used in the study of catalysts (Clausen *et al.*, 1991; Moggridge *et al.*, 1995; Revel *et al.*, 1999). These have regulated the flow and proportions of a mixture of gases using mass flow controllers to allow the *in situ* study of catalytic processes.

The furnace reported here is the first to be developed specifically for the analysis of silicate melts at temperatures up to 1773 K and under controlled fO_2s. Using this apparatus, accurate amounts of O_2

can be added or subtracted to change the redox state of species in the melt. To illustrate the use of the furnace, preliminary results for the oxidation state of Cr in a synthetic basaltic melt, similar to that found at mid-ocean ridges, are presented.

2. Experimental

The vertical tube furnace design is shown in Fig. 1. The furnace has a diameter of 75 mm, a height of 300 mm and weighs approximately 1.9 kg. It consists of a 10 mm ID (inner diameter) by 86 mm alumina tube heated by a bifilar $Pt_{0.6}/Rh_{0.4}$ wire wound over the central 22 mm. This central portion of the tube has an OD (outer diameter) of 14.5 mm while the remainder is 12.5 mm. The wire has a rectangular section (0.27 mm × 0.61 mm) and was wound into a 0.8 mm-deep and 1.5 mm pitch two-start groove machined into the outside of the tube. The ends of the wire were terminated by clamping into Cu rods that pass through insulated O-ring seals in the bottom of the furnace body. At the centre of the heater section this tube has two holes at 90° (3 mm and 5 mm in diameter) for entry and exit of incident and fluorescent X-rays; the heating wire is arranged to bypass these holes. A close-fitting 19 mm OD alumina tube surrounds the furnace tube and ensures that the winding remains in place. This outer tube is wrapped with a Pt foil heat shield, and is further shielded by a seven-turn open spiral scroll of Ni foil supported by 2 mm diameter radial alumina dowels. The whole heat-shield assembly is pierced by two holes, aligned with the holes in the alumina tube and the windows in the furnace body. The alumina tubes are held in position by fired pyrophyllite discs (16 mm thick) in the top and bottom of the furnace interior. The aluminium furnace body and lid are cooled by a water jacket.

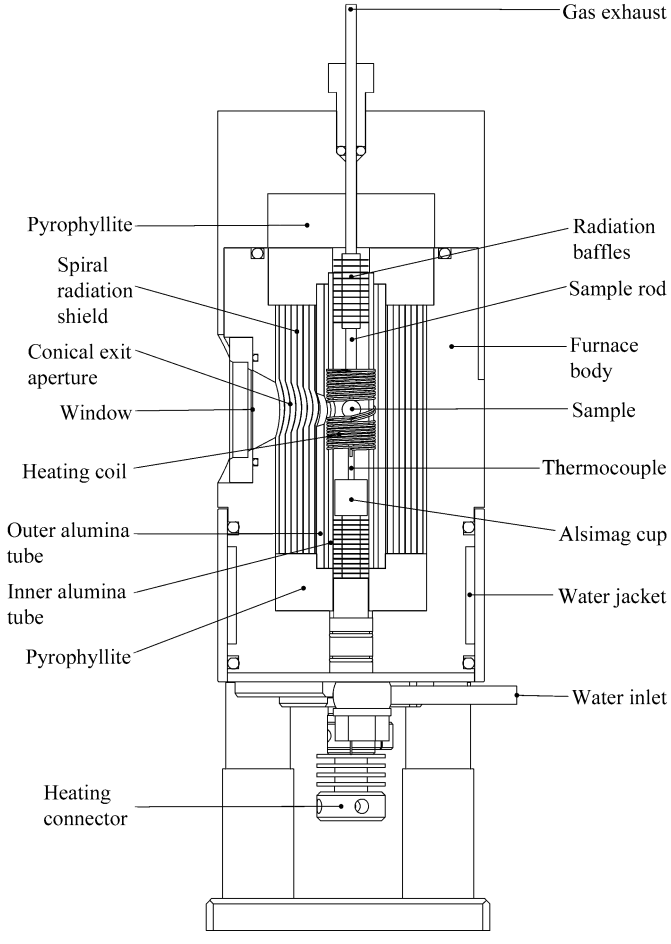

Figure 1
Cross section through the controlled oxygen fugacity X-ray spectroscopy furnace. The incident X-ray beam is perpendicular to the page.

Samples are suspended on loops of Pt wire or Re strip wrapped onto the end of a 2.9 mm OD alumina tube. Re can only be used at low fO_2s (Borisov & Jones, 1999) but is useful owing to the propensity of metal cations in a silicate melt (such as Fe and Cr) to alloy with Pt under these conditions. The molten samples are held on the loops by surface tension and the high viscosity of the melts. Solid samples may be suspended similarly using a Pt wire cage. A jig is used to ensure the front face of the sample is positioned on the axis of the furnace and at the correct height. The sample rod is collared by a series of Ni and Ir foil washers for heat shielding and is inserted through the removable lid and locked in position with an O-ring compression seal.

The furnace X-ray windows are made from aluminized 25 µm Kapton with the reflective layer facing the furnace interior. Aluminized mylar may also be used but is more prone to thermal degradation. The windows allow excellent X-ray transmission but almost no radiative heat loss. The entry window has a diameter of 6 mm to accommodate an incident beam of typically 1 mm × 2 mm. The diameter of the exit window (22 mm) is matched to the size of the aperture in the central tube and the solid-angle acceptance of an array detector positioned against the side of the furnace. The aperture sizes and furnace diameter were optimized for the diameter of the available detector. The windows were sealed to the furnace body with Viton O-rings.

Temperature is controlled by a Shinko FCS 23A programmable phase-angle controller supplying a step-down transformer with a maximum output of 40 V at 10 A. The control thermocouple is located against the inside wall of the alumina furnace tube. A second thermocouple is positioned centrally just below the sample. Both thermocouples are type B (Pt/Rh) and are supported by an axial four-bore 1.6 mm OD alumina tube. The top of this thermocouple tube is surrounded by an alsimag cup to catch any samples that might fall. The tube also supports Ni and Ir foil washers for thermal insulation. The temperature difference between that measured and the sample can be determined by mounting a non-alloying glass directly onto a thermocouple running down the inside of a calibration sample rod. The furnace is operable to at least 1773 K. The estimated accuracy of the sample temperature is within ±10 K; the uncertainty is due to the temperature gradient within the furnace, which is strongly dependent on the gas flow rate and variations in the sample position. The precision can be improved by using a constant flow rate for all experiments. The overall thermal stability of the system is better than ±1 K at 1673 K over time periods greater than 1 h.

The fO_2 or redox potential inside the furnace is imposed by CO/CO_2 gas mixtures using Tylan FC2900 mass-flow controllers. At high temperatures the ratio of CO and CO_2 accurately defines the partial pressure of oxygen according to the reaction $CO_2 \rightarrow CO + 0.5\ O_2$. Controllers with maximum flow rates of 10 and 200 standard $cm^3\ min^{-1}$ (SCCM) are used for both gases to ensure accuracy over extreme ratios. Typical total flow rates are around 10 SCCM. The gases are mixed with a frit filter before entering the furnace at the side through stainless-steel tubing. The gas occupies the entire furnace and exits through a central hole in the sample rod (effectively a sample tube), ensuring the gas flows past the sample. The furnace pressure is maintained slightly above atmospheric by an electronic exhaust control, comprising a solid-state pressure transducer and solenoid valve, that vents the toxic CO to an extraction line. This

valve closes when the furnace is evacuated to facilitate changing the sample gas environment. Gas changes were not attempted at high temperature owing to the danger of rupturing the window during evacuation. The furnace was cooled before undertaking an evacuation and filling procedure followed by reheating. Gas mixes equivalent to log fO_2s over a range from −3 to −13 at 1673 K (equivalent to approximately +3 to −7 relative to that defined by the coexistence of nickel and nickel oxide; the Ni/NiO buffer) can be used. The upper value is limited by oxidation of the Ni radiation baffles and the value of −3 corresponds to pure CO_2. The lower limit is determined by the corrosion of Pt arising from the absorption of C.

A schematic diagram detailing the furnace and associated instrumentation is given in Fig. 2.

Chromium *K*-edge XANES spectra were recorded at the Australian National Beamline Facility; beamline 20B (bending magnet) at the 2.5 GeV Photon Factory (KEK, Tsukuba, Japan). The excitation energy was selected using a water-cooled Si(111) channel-cut crystal monochromator located 11 m from the light source. The beam size of 2 mm (horizontal) × 1 mm (vertical) was controlled with a slit assembly 13 m from the source. Energy was calibrated by defining the first derivative peak of Cr in stainless steel foil to be 5989.2 eV. Fluorescence was measured using a Canberra GL0110S ten-element Ge array detector. The signal from each array element was passed from the detector, *via* a Canberra Model 2026XA spectroscopy amplifier (shaping time 0.25 µs), to a Canberra Model 2030 single-channel analyser which was set to pass the Cr K_α signal to the counting electronics. Peak counts due to Cr K_α photons were typically around 1500 per second per element with a total incoming count rate of less than 30000 per second per element, well within the linear response range of the detector system. The fluorescence was normalized to the incident beam flux monitored by an ionization chamber with a 30 cm path length containing 30% N_2 in He. Spectra were recorded from 5985 to 6025 eV using a 0.25 eV step size for a constant number of ionization chamber counts. Typical count times per point were around 5 s for a total scan time of 15–20 min. Following each scan, the signal from the ten detector elements was normalized and averaged to produce the reduced data for further analysis.

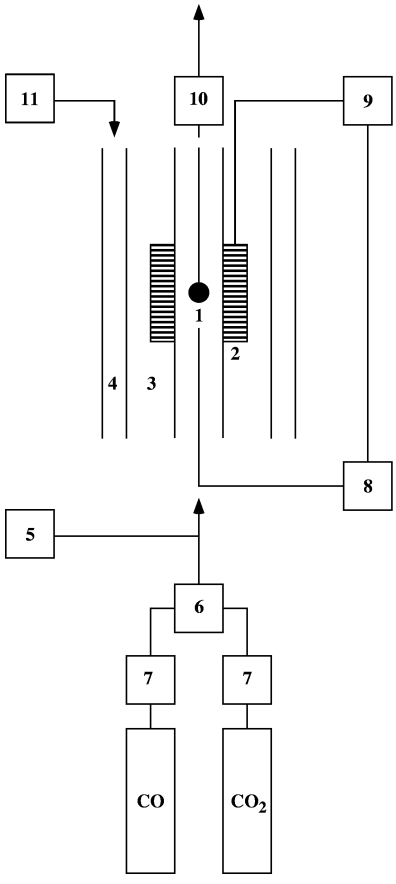

Figure 2
Schematic representation of the conceptual design and integration of the furnace system. 1: sample; 2: heating element; 3: thermal insulation; 4: water jacket; 5: vacuum pump; 6: frit gas-mixing filter; 7: mass flow controllers; 8: thermocouple; 9: temperature controller; 10: exhaust control; 11: water chiller.

After a change in temperature or fO_2, spectra were recorded as a function of time to determine when equilibration had been achieved. Temperature-dependent measurements were undertaken for a constant CO/CO_2 ratio.

Oxidation-state reference spectra were recorded at room temperature for Fe-free silicate melts of anorthite-diopside eutectic composition (42% $CaAl_2Si_2O_8$ + 58% $CaMgSi_2O_6$ by weight) to which was added 0.5 wt% Cr_2O_3, quenched in water to form glasses. Samples were equilibrated at 1673 K in a gas-mixing vertical tube furnace using CO/CO_2 and CO_2/O_2 mixtures to control the fO_2. The spectra shown are for samples equilibrated at log $fO_2 = -2$ (oxidized) and log $fO_2 = -14$ (reduced), under which conditions predominantly Cr^{3+} and Cr^{2+}, respectively, are expected (Berry & O'Neill, 2003; Schreiber & Haskin, 1976). The sample of simplified mid-ocean ridge basalt (MORB) composition (Niu & Batiza, 1993) was prepared from reagent-grade SiO_2 (52.0 wt%), Al_2O_3 (16.1 wt%), $CaCO_3$ = CaO (12.3 wt%), Fe_2O_3 = FeO (10.0 wt%), MgO (8.2 wt%), TiO_2 (1.3 wt%) and Cr_2O_3 (0.5 wt%). Alkali metals were not included owing to their volatility at atmospheric pressure. The liquidus of this composition is <1473 K for all the fO_2 conditions of this study. The MORB samples were pre-equilibrated at 1673 K and log $fO_2 = -8$.

3. Results

The Cr *K*-edge XANES spectra were normalized to the edge crest after subtraction of a constant baseline. Although it is more common to normalize spectra to fluorescence above the edge, crest normalization can be used as part of an empirical method for determining Cr oxidation states (Berry & O'Neill, 2003). The Cr^{2+} and Cr^{3+} quenched glass reference sample spectra (Fig. 3*a*) exhibit a shift in the energy of the main absorption edge with oxidation state and also a shoulder on the Cr^{2+} spectrum attributed to the $1s \rightarrow 4s$ transition. This transition is symmetry forbidden, but may gain intensity through orbital mixing in low-symmetry environments. The high-symmetry octahedral geometry favoured by Cr^{3+} results in this transition being weak or absent, whereas the transition becomes allowed in the Jahn–Teller distorted coordination common for Cr^{2+}. Owing to the fluid nature of a melt, Cr will adopt the coordination environment producing the greatest electronic stabilization. The $1s \rightarrow 4s$ feature is diagnostic of Cr^{2+} in a glass and may be used to quantify the Cr^{2+}/Cr^{3+} oxidation-state ratio (Berry & O'Neill, 2003). The $1s \rightarrow 3d$ pre-edge transition (particularly for Cr^{3+}, in which the e_g and t_{2g} components of the 3*d* state are resolved) is also observed. The energy of this transition in Fe has been used to quantify the Fe^{2+}/Fe^{3+} ratio (Bajt *et al.*, 1994; Wilke *et al.*, 2001; Berry *et al.*, 2003).

Spectra recorded for basaltic melt at 1673 K and various fO_2s (CO/CO_2 ratios; log $fO_2 = -6, -7, -8, -9, -10$) are shown in Fig. 3(*b*), and for a constant CO/CO_2 ratio but two different temperatures (1473, 1673 K) in Fig. 3(*c*). Spectra were also recorded at other

temperatures between 1473 and 1773 K but are not shown for clarity; in all cases the absorption edge shifts to lower energy with increasing temperature. For each experimental condition around five spectra of duration 15 min were recorded. Following changes in the CO/CO_2 ratio, the initial spectrum was usually significantly different from that recorded for the previous fO_2, but also different from the subsequent spectra. The third and further spectra were usually identical indicating that sample equilibrium had been attained with the gas mix (at least for the depth probed by the beam). The average of these spectra are shown. The system equilibrates more rapidly after a change in temperature with there being no discernible difference between the first and additional spectra. A room-temperature spectrum of the quenched basalt glass is also shown in Fig. 3(*c*). Spectra which are part of a series were not recorded systematically but rather in a random order to emphasize any changes that might occur due to the change in fO_2 or temperature.

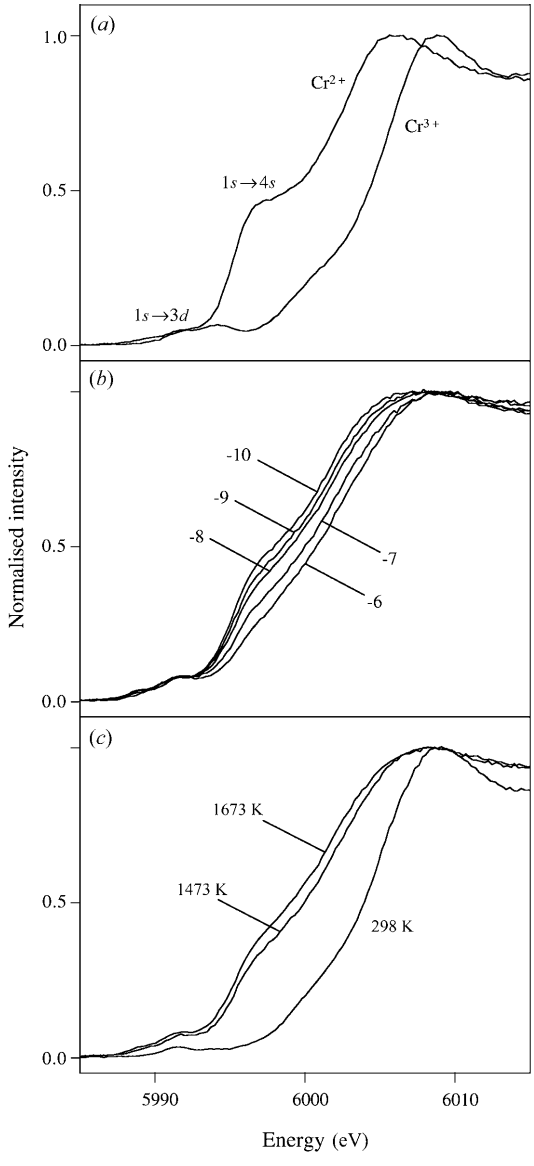

Figure 3
Cr *K*-edge XANES spectra for (*a*) anorthite-diopside glasses containing either Cr^{2+} or Cr^{3+}; (*b*) basaltic melt at 1673 K and the oxygen fugacity ($\log fO_2$) values indicated; and (*c*) basaltic melt as a function of temperature for a constant CO/CO_2 ratio, equal to $\log fO_2 = -8$ at 1673 K.

4. Discussion

The Cr^{2+} and Cr^{3+} Fe-free reference spectra (Fig. 3*a*) are the end members of a series of glasses prepared as a function of fO_2. XANES spectra have been recorded for 20 samples equilibrated at 1673 K and values of $\log fO_2$ ranging from 0 to −14. Cr is the only redox variable element in this composition and systematic changes in the Cr *K*-edge spectrum with fO_2 must reflect changes in the Cr oxidation-state ratio. With decreasing fO_2, the edge shifts to lower energy and the $1s \rightarrow 4s$ edge shoulder gains intensity. The area of the $1s \rightarrow 4s$ feature in the derivative spectrum can be used to quantify the Cr^{3+}/Cr^{2+} ratio and the results obey the theoretical expression $\log[Cr^{3+}/Cr^{2+}] = 0.25 \log fO_2 + C$, derived from the reaction $Cr^{2+}O + 0.25\ O_2 = Cr^{3+}O_{1.5}$ (Berry & O'Neill, 2003). This is strong evidence that the glasses contain known Cr^{3+}/Cr^{2+} ratios and that the fO_2 end members provide Cr^{2+} and Cr^{3+} model compound spectra. The glasses also exhibit colours characteristic of Cr^{2+} (blue) and Cr^{3+} (green). There was no evidence of quench microcrystals by either optical microscopy or backscattered electron imaging, while the $\log fO_2$ of the most reduced sample is still several orders of magnitude more oxidizing than that required for the precipitation of Cr metal. The glass composition, temperature and $\log fO_2$s are all similar to the experiments of Schreiber & Haskin (1976) in which Cr^{2+} was identified by wet chemistry and electron paramagnetic resonance spectroscopy. Reference glasses such as those presented here represent ideal model compounds since for similar glasses the effect of the coordination environment is minimized.

The energy of the edge shift and intensity of the shoulder in the high-temperature Fe-bearing basaltic melt spectra shown in Fig. 3(*b*) suggest a significant contribution from Cr^{2+}. The changes in the spectra with $\log fO_2$ at constant temperature are indicative of changes in the oxidation state of Cr and the energy shift and shoulder appear associated with Cr^{2+} as in the reference glass. The presence of Cr^{2+} at these values of $\log fO_2$ is consistent with our results for Fe-free glasses (Berry & O'Neill, 2003). Although the redox state of Fe will also vary with the fO_2, the change in $Fe^{3+}/\Sigma Fe$ is sufficiently small such that any resulting change in melt structure is unlikely to have a significant affect on the Cr coordination and thus the edge spectrum. The $\log fO_2$ dependence of the Cr^{2+}-like features also confirms that they are not a consequence of the increase in temperature or molten state. Increases in temperature increase the Cr^{2+} character of the spectra (Fig. 3*c*) and, in the absence of the fugacity data, it may not be possible to distinguish the appearance of Cr^{2+} from the possible effect of temperature on the Cr^{3+} spectrum. For example, the spectral changes could have been attributed to the $1s \rightarrow 4s$ transition of Cr^{3+} arising from high-temperature distortions to the coordination environment. The differences in the spectra between 1473 and 1673 K may be a temperature effect but are more likely to truly reflect an increase in the Cr^{2+} content. This is consistent with a previous determination of Cr oxidation states at two temperatures (Schreiber & Haskin, 1976) and the results of sub-solidus phase equilibria experiments (Li *et al.*, 1995).

These *in situ* experiments illustrate that it is possible to directly monitor changes in XANES spectra as a function of temperature and fO_2 that correlate with changes in the oxidation-state ratio. This identifies Cr^{2+} in a Fe-bearing basaltic melt under geological conditions. At 1673 K upper mantle redox conditions span the $\log fO_2$ range from approximately −10 (Fe/FeO) to −6 (Ni/NiO). It is estimated that at 1673 K and $\log fO_2 = -8$ around half the total Cr is present as Cr^{2+} (Berry & O'Neill, 2003). The spectrum of melt quenched to a glass under these conditions (Fig. 3*c*), however, only indicates the presence of Cr^{3+}. Cr^{2+} has never been identified in a

terrestrial material and there is no evidence of this oxidation state in our experiments on basalt quenched from any fO_2 relevant to the crust or upper mantle. Only when quenching from extremely reducing conditions can Cr^{2+} be observed. We suggest that Cr^{2+} oxidizes to Cr^{3+} in the presence of Fe^{3+} on cooling, according to the reaction $Cr^{2+} + Fe^{3+} \rightarrow Cr^{3+} + Fe^{2+}$. In basalt any changes in the Fe oxidation-state ratio associated with this reaction are not expected to be seen owing to the small amount of Cr relative to Fe. In terrestrial magmas the fO_2 and Fe concentration are such that the net amount of Fe^{3+} (Sack *et al.*, 1980; Canil *et al.*, 1994) is sufficient to remove Cr^{2+} from the system on cooling. This Cr/Fe redox interaction explains why all Cr occurs as Cr^{3+} in terrestrial basalts (which contain Fe^{3+}/Fe^{2+}), while the absence of Fe^{3+} in the more reducing lunar environment enables Cr^{2+} to persist in quenched glasses. The stabilization of Cr^{2+} with increasing temperature may also explain the high solubility of Cr in high-temperature mantle melts (*e.g.* komatiites) owing to the suppression of accessory mineral (*e.g.* $FeCr_2^{3+}O_4$) crystallization (Liang & Elthon, 1990).

5. Conclusions

This work provides the first direct evidence for the importance of Cr^{2+} in terrestrial basaltic magmas. Although circumstantial evidence for the stability of Cr^{2+} in silicate melts can be derived from phase-equilibrium studies, no method has been available previously to determine the oxidation state of Cr in the presence of Fe. The oxidation of Cr^{2+} to Cr^{3+} on cooling in Fe-bearing systems explains why Cr^{2+} has not been found in natural samples. These results could only be obtained by *in situ* high-temperature XANES spectroscopy. The controlled-atmosphere spectroscopy furnace described is ideal for this purpose but also sufficiently versatile to be used with almost any geological material over the entire temperature and fO_2 range of the Earth's crust and upper mantle.

The XANES experiments were performed at the Australian National Beamline Facility with support from the Australian Synchrotron Research Program, which is funded by the Commonwealth of Australia under the Major National Research Facilities Program. We would like to thank W. O. Hibberson, J. Hermann and U. Faul for assistance with the operation of the furnace at various times. AJB also thanks the Australian Research Council for the award of a Fellowship.

References

Bajt, S., Sutton, S. R. & Delaney, J. S. (1994). *Geochim. Cosmochim. Acta*, **58**, 5209–5214.
Barnes, S. J. (1986). *Geochim. Cosmochim. Acta*, **50**, 1889–1909.
Berry, A. J. & O'Neill, H. St. C. (2003). *Am. Mineral.* Submitted.
Berry, A. J., O'Neill, H. St. C., Jayasuriya, K. D., Campbell, S. J. & Foran, G. J. (2003). *Am. Mineral.* In the press.
Borisov, A. & Jones, J. H. (1999). *Am. Mineral.* **84**, 1528–1534.
Canil, D., O'Neill, H. St. C., Pearson, D. G., Rudnick, R. L. & McDonough, W. F. (1994). *Earth Planet. Sci. Lett.* **123**, 205–220.
Clausen, B. S., Steffensen, G., Fabius, B., Villadsen, J., Feidenhans'l, R. & Topsøe, H. (1991). *J. Catal.* **132**, 524.
Crozier, E. D., Lytle, F. W., Sayers, D. E. & Stern, E. A. (1977). *Can. J. Chem.* **55**, 1968–1973.
Dent, A. J., Greaves, G. N., Roberts, M. A., Sankar, G., Wright, P. A., Jones, R. H., Sheehy, M., Madill, D., Catlow, C. R. A., Thomas, J. M. & Rayment, T. (1995). *Nucl. Instrum. Methods Phys. Res. B*, **97**, 20–22.
Farges, F., Brown, G. E. Jr, Calas, G., Galoisy, L. & Waychunas, G. A. (1994). *Geophys. Res. Lett.* **21**, 1931–1934.
Farges, F., Brown, G. E. Jr, Navrotsky, A., Gan, H. & Rehr, J. R. (1996). *Geochim. Cosmochim. Acta*, **60**, 3055–3065.
Farges, F., Flank, A.-M., Lagarde, P. & Ténégal, F. (1999). *J. Synchrotron Rad.* **6**, 193–194.
Farges, F., Itié, J.-P., Fiquet, G. & Andrault, D. (1995). *Nucl. Instrum. Methods Phys. Res. B*, **101**, 493–498.
Filipponi, A. (2001). *J. Phys. Condens. Matter*, **13**, R23–R60.
Filipponi, A., Borowski, M., Bowron, D. T., Ansell, S., Di Cicco, A., De Panfilis, S. & Itiè, J.-P. (2000). *Rev. Sci. Instrum.* **71**, 2422–2432.
Hanson, B. & Jones, J. H. (1998). *Am. Mineral.* **83**, 669–684.
Hilbrandt, N. & Martin, M. (1999). *J. Synchrotron Rad.* **6**, 489–491.
Hoser, A., Hilbrandt, N., Martin, M. & Denecke, M. (1995). *Physica B*, **208/209**, 321–322.
Jackson, W. E., Mustre de Leon, J., Brown, G. E. Jr, Waychunas, G. A., Conradson, S. D. & Combes, J.-M. (1993). *Science*, **262**, 229–233.
Jacobs, G., Egry, I., Maier, K., Platzek, D., Reske, J. & Frahm, R. (1996). *Rev. Sci. Instrum.* **67**, 3683–3687.
Launay, X., Landron, C., Coutures, J. P. & Bazin, D. (1997). *J. Phys.* **7**, 1255–1256.
Li, J.-P., O'Neill, H. St. C. & Seifert, F. (1995). *J. Petrol.* **36**, 107–132.
Liang, Y. & Elthon, D. (1990). *Nature (London)*, **343**, 551–553.
Lytle, F. W., Wei, P. S. P. & Greegor, R. B. (1979). *J. Chem. Phys.* **70**, 4849–4855.
Moggridge, G. D., Schroeder, S. L. M., Lambert, R. M. & Rayment, T. (1995). *Nucl. Instrum. Methods Phys. Res. B*, **97**, 28–32.
Murck, B. W. & Campbell, I. H. (1986). *Geochim. Cosmochim. Acta*, **50**, 1871–1887.
Niu, Y. & Batiza, R. (1993). *J. Geophys. Res.* **98**, 7887–7902.
Poustovetov, A. A. & Roeder, P. L. (2000). *Can. Mineral.* **39**, 309–317.
Revel, R., Bazin, D., Seigneurin, A., Barthe, P., Dubuisson, J. M., Decamps, T., Sonneville, H., Poher, J. J., Maire, F. & Lefrancois, P. (1999). *Nucl. Instrum. Methods Phys. Res. B*, **155**, 183–188.
Roeder, P. L. & Reynolds, I. (1991). *J. Petrol.* **32**, 909–934.
Sack, R. O., Carmichael, I. S. E., Rivers, M. & Ghiorso, M. S. (1980). *Contrib. Mineral. Petrol.* **75**, 369–376.
Schreiber, H. D. & Haskin, L. A. (1976). *7th Proc. Lunar Sci. Conf.* pp. 1221–1259.
Sutton, S. R., Jones, K. W., Gordon, B., Rivers, M. L., Bajt, S. & Smith, J. V. (1993). *Geochim. Cosmochim. Acta*, **57**, 461–468.
Waychunas, G. A. (1987). *Am. Mineral.* **72**, 89–101.
Waychunas, G. A., Apted, M. J. & Brown, G. E. Jr (1983). *Phys. Chem. Miner.* **10**, 1–9.
Waychunas, G. A., Brown, G. E. Jr, Ponader, C. W. & Jackson, W. E. (1988). *Nature (London)*, **332**, 251–253.
Wilke, M., Farges, F., Petit, P.-E., Brown, G. E. Jr & Martin, F. (2001). *Am. Mineral.* **86**, 714–730.
Wong, J., Lytle, F. W., Messmer, R. P. & Maylotte, D. H. (1984). *Phys. Rev. B*, **30**, 5596–5609.